ISSN 1063-7834, Physics of the Solid State, 2014, Vol. 56, No. 2, pp. 302–309. © Pleiades Publishing, Ltd., 2014.
Original Russian Text © G.S. Patrin, I.A. Turpanov, A.V. Kobyakov, D.A. Velikanov, K.G. Patrin, L.A. Li, V.K. Mal'tsev, S.M. Zharkov, V.I. Yushkov, 2014, published in Fizika Tverdogo Tela, 2014, Vol. 56, No. 2, pp. 301–307.

MAGNETISM

Synthesis and Magnetic States of Cobalt in Three-Layer Co/Ge/Co Films

G. S. Patrin[a, b], I. A. Turpanov[a], A. V. Kobyakov[b], D. A. Velikanov[a, b], K. G. Patrin[a, b], L. A. Li[a], V. K. Mal'tsev[a], S. M. Zharkov[a], and V. I. Yushkov[a, b]

[a] *Kirensky Institute of Physics, Siberian Branch of the Russian Academy of Sciences, Akademgorodok 50–38, Krasnoyarsk, 660036 Russia*

[b] *Institute of Engineering Physics and Radio Electronics, Siberian Federal University, ul. Kirenskogo 28, Krasnoyarsk, 660074 Russia*

e-mail: nanonauka@mail.ru

Received July 8, 2013

Abstract—The magnetic properties of three-layer Co–Ge magnetic films have been studied experimentally as a function of technological conditions of their deposition. It has been found that the films deposited at a high deposition rate have a granular structure, and the films obtained at a low deposition rate have an X-ray amorphous structure. Electron microscopy and nuclear magnetic resonance studies have demonstrated that, at the same cobalt layer thickness, the semiconductor granule sizes depend on the average semiconductor layer thickness and correlate with the formation of different cobalt phases (amorphous, cubic, and hexagonal). The thermomagnetic properties of the films have been investigated.

DOI: 10.1134/S1063783414020255

1. INTRODUCTION

Recently, ferromagnetic metal–semiconductor films are of a noticeable interest [1]. First, this is due to the existence of a semiconductor component. In multilayer magnetic films with a semiconductor interlayer, the ferromagnetic layers interact with each other via the electron subsystem of the semiconductor layer. In this case, the current carrier concentration and, as a result, interlayer interactions can be controlled by external actions. By now, different interactions have been revealed in films with a semiconductor interlayer: the temperature-dependent interlayer exchange [2], unusual behavior of the interlayer interaction as a function of the thicknesses of nonmagnetic [3, 4] and magnetic [5] interlayers, and the behavior similar to the spin-glass behavior [6]. In addition, the possibility arises of controlling the magnetic and resistive properties of the structure by choosing the method of stacking structural layers and choosing the semiconductor material. All these studies are aimed at designing new film structures and searching for the effects that are promising for their use in spintronic devices. One of such effects is the giant magnetoresistance effect, and heterogeneous materials are very promising for this direction.

The most abundant component of heterogeneous structures demonstrating this effect is cobalt. The reason is its band character of the magnetism that brings about a high spin polarization of conduction electrons and, at the same time, the itinerant character of 3*d* electrons provides a substantial transformation of the cobalt magnetism in the compounds (the charge transfer effect) [7].

Among semiconductors, germanium exhibits the most pronounced properties (electrons and holes have a high mobility, long lifetime, large mean free path, and small band gap.

However, film structures based on a 3*d* metal–semiconductor system are very sensitive to technological conditions (for example, in the Fe/Si structure, the interlayer interaction sign is changed depending on the substrate temperature with other conditions being the same [8]).

Thus, the aim of this work is to reveal the correlation between the technological conditions (deposition rate, choice of the thickness, and so on) and the formation of the magnetic state of Co/Ge/Co films, which have been poorly studied [6].

2. SAMPLE PREPARATION AND EXPERIMENTAL TECHNIQUES

We synthesized Co/Ge/Co films with different nonmagnetic layer thicknesses averaged over the film area. The films were obtained by ion-plasma spraying at a base pressure $P = 10^{-6}$ Torr in argon atmosphere. We used glass as a substrate material, and the substrate temperature during deposition was $T \approx 373$ K.

It is known [8] that, at the thicknesses $t^* \leq 5.0$ nm, the cobalt magnetization decreases markedly with decreasing cobalt film thickness, and the deposition rate influences the layer material structure. Because of

this, we synthesized and studied two series of the films with $t_{Co} \gg t^*$. Series I: $t_{Co} = 13 \pm 0.3$ nm, the germanium film thickness was variable; the deposition rate was 0.15 nm/s for cobalt and 0.12 ± 0.02 nm/s for germanium. Series II: $t_{Co} = 15 \pm 0.3$ nm, the germanium film thickness was variable; the deposition rate was 0.15 Å/s for cobalt and 0.12 ± 0.02 Å/s for germanium. The average thicknesses of germanium and cobalt were found by X-ray spectroscopy. The electron microscopy studies of the films were performed on a PREM-200 transmission electron microscope. The top view image from a film region was photographed by a camera fitted into a microscope. The film surface structure was studied on a Veeco Multi Mode atomic force microscope (resolution of ~1 nm). The magnetic data were obtained using a SQUID magnetometer operating in the temperature range $T = 4.2$–300 K and in magnetic fields $H \le 800$ Oe in the geometry where the magnetic field was aligned with the film plane. Before each of the measurements, the film was first placed into a demagnetizer and, then, cooled in a zero magnetic field (ZFC mode). It is known [9] that the absorption line intensity at magnetic resonance (determined as the area under the resonance curve) is proportional to the number of absorption centers. Since each of the magnetic cobalt phases has a proper frequency range, the cobalt phase composition in the films was determined also using a nuclear magnetic resonance (NMR) spectrometer. The NMR spectra were measured by a two-pulse spin–echo technique. The operating frequency range was $\omega_{HF} = 150$–240 MHz. The probe high-frequency magnetic field pulse width was 0.1–1.0 μs, and the interval between pulses was 4–5 μs. The electrical resistance was measured by the four-probe method.

3. EXPERIMENTAL RESULTS

3.1. Electron Microscopy

The electron microscopy studies show that the microstructure of I type films contains grey and white fine particles (Figs. 1a–1d). As is seen that the microdiffraction patterns from the regions with the white formations and without them are completely identical in the set of diffraction reflections and their intensity. The electron diffraction patterns have a shape of broadened polycrystalline rings. The interpretation of the electron diffraction patterns shows that the magnetic layers consist of phase mixtures. For example, we can say with confidence that the film with $t_{Ge} = 1.9$ nm (Figs. 1a, 1b) contains the face-centered cubic phase (fcc) of cobalt, since we observe rather intense reflections at $d = 0.107$, 0.125, and 0.205 nm (JCPDS card No. 15-0806), and also a low amount of the hexagonal close-packed (hcp) cobalt, since we see a weak reflection at $d = 0.192$ nm and, it is possible, a broadened and shifted reflection at $d = 0.2165$ nm (JCPDS card No. 05-0727). There is also a diffuse reflection which we centered at $d = 0.262$ nm. It can be assigned to a modified phase of the CoGe compound or, what is thought to be more probable, to a superposing the reflections from X-ray amorphous phases of cobalt to germanium. We did not observed in this film of clear reflections inherent in the crystalline α-Ge.

In other limiting case with $t_{Ge} = 11$ nm (Figs. 1c and 1d), reflections are more intense, but their number is small. Apparently, the reflections with $d = 0.146$ and 0.242 nm can be assigned to the hcp phase, and the intensive halo centered at $d = 0.107$ nm is related to the existence of the α-Ge phase. The halo with $d = 0.198$ nm is formed due to α-Ge and due to a mixture of cobalt phases. The assumption on the mixture of cobalt phases based on the fact that the diffraction reflection center is in the middle between the positions between the highest-intense reflections $d_{111} = 0.2047$ nm (fcc phase) and $d_{101} = 0.191$ nm (hcp phase). This is, with increasing layer thickness, equilibrium phases begin to prevail in it, i.e., the hexagonal phase in the cobalt film, and the cubic phase in the germanium film.

In the cases when germanium thickness varies in a series $1.9 \longrightarrow 11$ nm, the electron diffraction pattern varies so that the granularity in cobalt becomes clearer, and, in this case, granules coalesce.

The electron microscopy data for films of the II type ($t_{Co} = 15.0$ nm) are shown in Figs. 1e–1h. In this case, in parallel to deposition of the three-layer film structure, the control layers of each of the elements were deposited during the same cycle. It is seen that microstructures of the layers are almost homogeneous. Cobalt layer is predominantly the hexagonal phase (lattice parameters are $a = 2.503$ Å and $c = 4.0605$ Å). This follows from the fact that we observe almost complete set of reflections characteristic of the cobalt hcp phase with structure $P6_3/mmc$; however, since the rings are noticeably broadened and overlapped (Fig. 1f, the crystallite sizes are likely very small (discussed slightly below), and the pattern is close to X-ray amorphous structure. The germanium layer (Fig. 1h) clearly demonstrates the cubic α-phase with the $Fd3m$ structure (lattice parameter $a = 5.6576$ Å).

3.2. Atomic Force Microscopy

Figure 2 shows the micrographs of the cobalt upper surface immediately after deposition of films of both types. It is seen that the roughness and, correspondingly, the granule sizes differ substantially depending on the deposition rate. In the case of the films of the type I, the heterogeneity sizes are approximately one to two orders of magnitude higher than that in the films of the II type. The average grain size of the latter is $d \approx 0.84$ nm. We see that, at low layer deposition rate, the heterogeneity sizes are such that the film can actu-

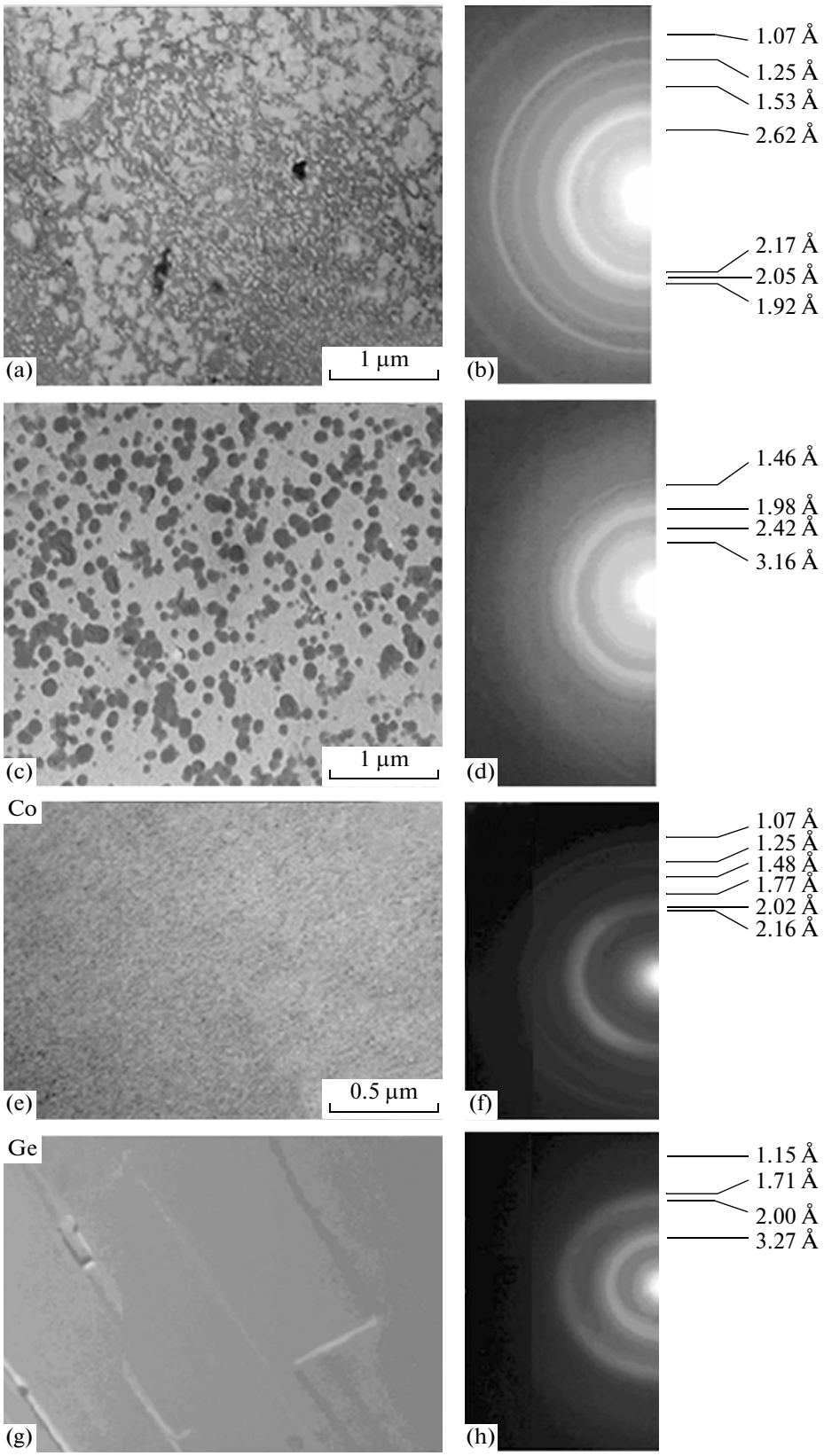

Fig. 1. (a, c, e, g) Enlarged micrographs of film regions (top view) and (b, d, f, h) electron microdiffraction patterns of the same regions, respectively. The electron microdiffraction patterns were obtained from (ad) Co/Ge/Co films (series I) and (e–h) the first cobalt layer and germanium (series II), respectively.

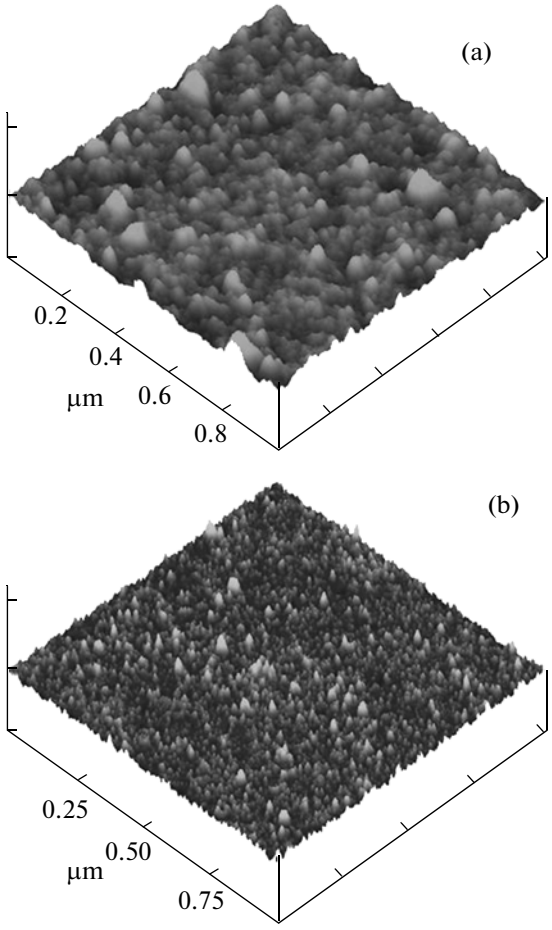

Fig. 2. Atomic force microscopy of Co/Ge/Co films prepared at (a) high deposition rate (series I) and (b) low deposition rate (series II).

ally be considered as that consisting of microgranules such that the structure can be considered as an X-ray amorphous. The data on the atomic force and electron microscopies correlate to each other.

Cobalt and germanium phases in the Co/Ge/Co films with variable layer thicknesses according to NMR studies

Co/Ge/Co		Co-phases			Ge-phases
$t_{Co} = 13$ nm	$t_{Ge} \approx 2.5$ nm	am	fcc		am
	$t_{Ge} \approx 5.8$ nm	am	fcc		am
	$t_{Ge} \approx 7.5$ nm		fcc	hcp	fcc
$t_{Co} = 15$ nm	$t_{Ge} \approx 2.5$ nm			hcp	am
	$t_{Ge} \approx 7.5$ nm			hcp	fcc

The fcc phase has a line in the range $\omega_{HF} = 210$–213 MHz; the hcp phase has a line in the range $\omega_{HF} = 215$–217 MHz; and the amorphous phase has absorption at frequencies $\omega_{HF} < 210$ MHz.

3.3. NMR Data

Our NMR studies show that the NMR spectrum of the films synthesized is a complex asymmetric line that can be considered as a superposition of the Lorentzian-type lines. Each of the cobalt phases is known to have a proper individual NMR spectrum. For example, depending on the synthesis conditions and the structural features, the fcc phase has a line in range $\omega_{HF} = 210$–213 MHz, the hcp-phase in range $\omega_{HF} = 215$–217 MHz, and the amorphous phase has an absorption at frequencies $\omega_{HF} < 210$ MHz [10]. Based on these frequency intervals, we expanded the experimental NMR curve into the components, and the results of fitting are shown in Fig. 3: curve *1* is the fcc-phase spectrum; curve *2* is the amorphous phase spectrum; and curve *3* is the hcp phase spectrum. In addition, the data of the NMR studies are given in table. From Fig. 3, it is seen that, in the case $t_{Co} = 13$ nm and $t_{Ge} \approx 2.5$ nm, as in the films with $t_{Co} = 13$ nm studied in [11] (Fig. 3a), the film consists of a mixture of the amorphous and cubic phases; further increase in the germanium film thickness leads to the formation of the hexagonal phase (Fig. 3b), and, at one more higher t_{Ge}, when germanium takes the cubic structure (Fig. 3c), the amorphous phase disappears, and only a mixture of the cubic and hexagonal phases is retained. As was found earlier [11], the increase in the magnetic Co layer thickness brings about the decrease in the fraction of the metastable amorphous and cubic phases and the increase in the fraction of the hexagonal phase. This regularity is also observed in the films with $t_{Co} = 15.0$ nm (Figs. 3d–3f). However, we see here that the cobalt amorphous phase is observed still at $t_{Ge} = 2.5$ nm (Fig. 3d); then, with increasing area-average germanium film thickness (and the transition of germanium to the amorphous phase), the Co amorphous phase disappears, the hexagonal phase is formed, and its fraction with respect to the cubic phase increases (Figs. 3e and 3f). Thus, the NMR experiments confirm the conclusions of the electron microscopy studies on the existence of several magnetic phases in the films.

In the case of films of the II type, there is one broadened line inherent in the hcp phase and slightly shifted toward lower frequencies.

This behavior is immediately reflected on the film magnetic characteristics.

3.4. Magnetic Properties

Temperature dependences of the magnetization ($M(T)$) of series I films with $t_{Co} = 13$ nm and $t_{Ge} = 2.5$ and 5.8 nm measured in different magnetic fields are identical to the films with $t_{Co} = 12.5$ nm and $t_{Ge} = 2.5$ and 5.8 nm [11]. All the dependences were obtained in the ZFC regime and presented in Fig. 4. It is seen that the temperature dependences of the magnetization films have a thermoactivation character for all non-

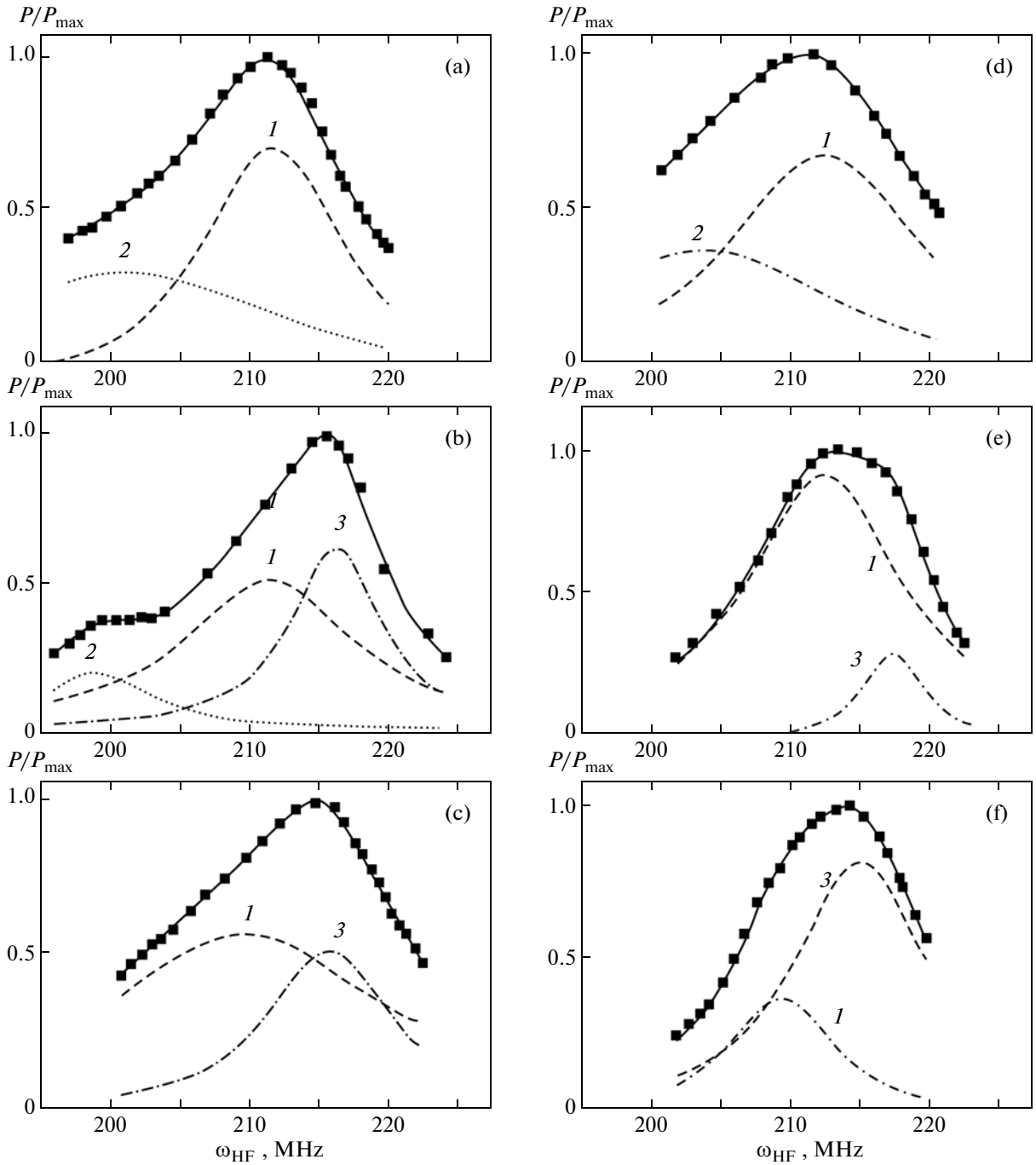

Fig. 3. NMR spectra of Co/Ge/Co films with (a–c) t_{Co} = 12.5 nm and (d–f) t_{Co} = 15.0 nm for t_{Ge} = (a) 2.5, (b) 4.0, (c) 7.0, (d) 2.5, (e) 5.5, and (f) 7.5 nm. Points are experimental data, and lines are the results of fitting.

magnetic layer thicknesses under study. In weak magnetic fields, there is the "blocking" temperature (T_b) lower which the magnetization is close to zero. The magnetization begins to markedly increase, only when the temperature becomes higher than some temperature depending on the measuring field. The magnetization reaches the value corresponding to the magnetization on the field dependence for given magnetic field. Figure 4 shows that the blocking temperature of the film with t_{Ge} = 2.5 nm is lower than that for the film with t_{Ge} = 5.8 nm; in this case, the film with small germanium thickness is saturated in lower fields.

The field dependences of the magnetization are shown in Fig. 5. The magnetization curve of the films from series I (Fig. 5a) with t_{Ge} = 2.5 nm is flattened in fields ~600 Oe, while in the case t_{Ge} = 5.84 nm, the saturation is reached in fields ~1600 Oe. For the films of

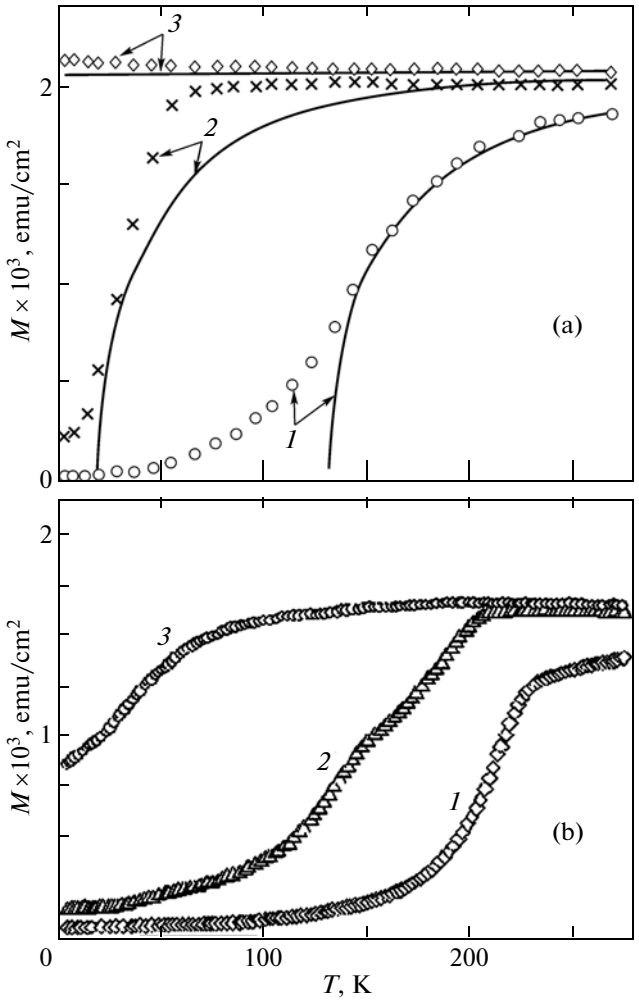

Fig. 4. Temperature dependences of the magnetization of Co/Ge/Co films with $t_{Co} = 13.0$ nm and $t_{Ge} =$ (a) 2.5 and (b) 5.8 nm measured in magnetic fields $H =$ (*1*) 50, (*2*) 200, and (*3*) 800 Oe.

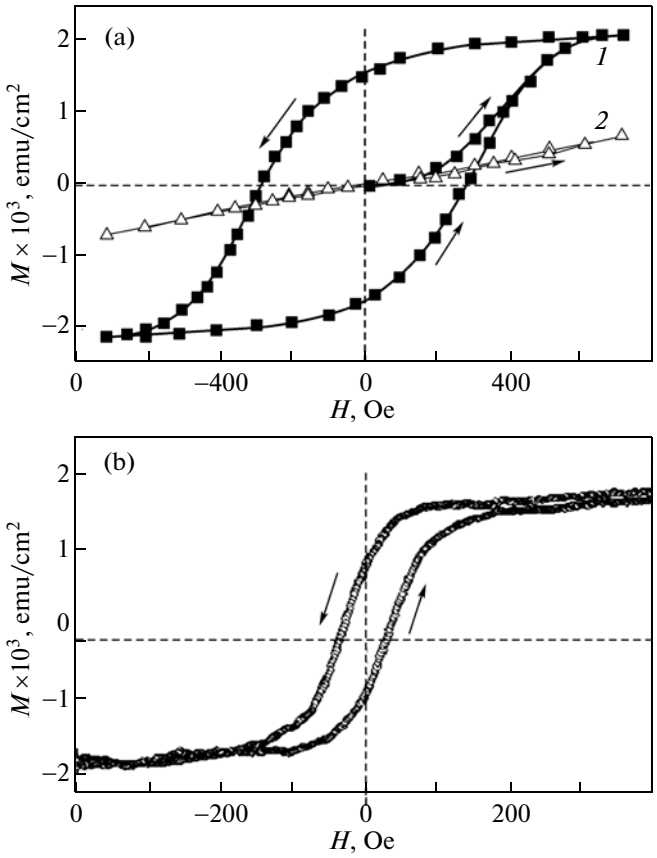

Fig. 5. Field dependences of Co/Ge/Co films: (a) series I with $t_{Ge} =$ (*1*) 2.5 and (*2*) 5.8 nm and (b) series II with $t_{Ge} = 3.6$ nm.

series II, the saturation field is approximately ~200 Oe (Fig. 5b). All films of both series have the same value of the magnetization saturation (~2×10^{-3} emu/cm^2). Specific measurements of the influence of the germanium structure on the cobalt coercivity have not been performed. It is the next problem of studying Co/Ge films.

4. DISCUSSION OF THE RESULTS

As follows from the NMR data for the film of series I with $t_{Ge} = 2.5$ nm (Fig. 3b), the hexagonal germanium fraction is small (<10%), and because of this, the phase can be considered in an impurity limit and assume that granules do not interact to each other. For such situation the model was proposed [12], in which strongly anisotropic particles are distributed in an isotropic matrix and related to it by exchange interaction. In terms of this model, the energy of the film system is

$$E = -tM_0H\cos\varphi - H\sum_j \mu_j\cos\alpha_j - \lambda M\sum_j \mu_j\cos(\varphi - \alpha_j) - \sum_j D_j\cos^2(\Theta_j - \alpha_j), \quad (1)$$

where $M_0 = M_0(H)$ is the magnetization in the given magnetic field; φ is the angle determining the magnetization direction; α_j is the angle between the magnetic moment of the jth granule and the external field; $\mu_j = \mu_j(H, T)$ is the granule magnetic moment; λ is the constant of the exchange interaction between the granule and the matrix; D_j is the magnetic anisotropy constant of the granule; and t is the effective thickness of the magnetic layer. This problem was solved in the assumption that the magnetic anisotropy in small magnetic fields is much higher than the Zeeman energy and the interaction energy between the matrix and the granule ($D_j \gg \{H\mu_j, \lambda M\mu_j\}$). From the condi-

tion of the minimum of Eq. (1), we obtained the relationship for the magnetization:

$$M = 2t - M_s\sqrt{1-\left(\frac{qm(T)(\sin\varphi(T,H))}{(1-q)M_0(H)}\right)^2}, \quad (2)$$

where

$$\langle \sin\varphi(T,H)\rangle = \frac{1}{\mu_0(T)}\int_0^{\pi/2}\mu(T,H,\theta)\sin^2\theta d\theta$$

and

$$\mu_0(T) = m(T)\frac{4\pi}{3}r^3. \quad (3)$$

Here, $m(T)$ is the magnetization of the granule material; r is the granule radius; q is the hexagonal phase fraction, and the integration is performed over the upper hemisphere.

This approach was used to analysis of the magnetic behavior of the film with $t_{Ge} = 2.5$ nm.

The results of the numerical calculation are shown in comparison with the experimental dependences in Fig. 4 (panel (a), solid curves).

In the calculations, the adjustable parameters were exchange interaction constant λ and particle radius r. It was obtained that $\lambda = 0.1$ and $r = 1.91$ nm, and other parameters were taken from the experimental dependences. We observe good agreement the experiment and the theory, exception for "tails" in the transition temperature range. However, this is related to a roughness of the used molecular field approximation, where the magnetic structure heterogeneities are not taken into account.

We did not obtain such a good fitting for the film with $t_{Ge} = 5.8$ nm. As is seen from Fig. 3c, the hexagonal phase fraction is significantly higher than the cubic phase fraction. In this case, we are beyond the impurity approximation, and, it is like, it is necessary to include the formation of conglomerates from hexagonal cobalt granules due to coalesce of the granules and to take into account the exchange interaction between the granules. This can explain the higher value of the saturation field and more complex temperature dependence of the magnetization (e.g., the inflection in curve *2* in Fig. 4b). The most substantial difference in the behavior is observed in the field dependences of the magnetization. The film containing impurity hexagonal cobalt granules have a closed hysteresis loop in fields $H \le 500$ Oe, while, in the film mainly consisting of the granular hexagonal cobalt, this region corresponds to the initial segment of the magnetization curve. This behavior can be explained, taking into account [13] that the magnetic particle anisotropy increases by higher than an order of magnitude in going to the nanometer scale as compared to the bulk material. This is, the film with $t_{Ge} = 5.8$ nm is an ensemble of hexagonal cobalt particles of strongly anisotropic, chaotically oriented and interacting to each other, and, against this background, the cubic cobalt does not give substantial contribution.

The results obtained for the films of series II are described in the framework of the standard approach, and it is not necessary to use new concepts for the explanation. As is seen from Figs. 1e–1h and Fig. 2b, the film structure is fine-grained to an extent that it can be considered as a continuous film. As temperature is changed, the magnetization obeys to the "$T^{3/2}$" law, and the field dependence corresponds to the behavior of cobalt material.

5. CONCLUSIONS

As a result of the performed experimental studies, it was found that, depending on technological conditions of preparing films, the structure and state of the magnetic cobalt layer substantially depend on the germanium state (amorphous or cubic semiconductor) at the metal–semiconductor interface.

At $t_{Ge} < 2.5$ nm (amorphous Ge phase), Co has the amorphous phase. At large Ge thicknesses (transition to the cubic phase), the hexagonal Co phase is formed, and its fraction increases relative to the cubic phase. Since the anisotropy field of hexagonal cobalt is higher than that of cubic cobalt, the magnetization is saturated at lower fields at small germanium and cobalt thicknesses.

The choice of the deposition rate and germanium thickness allows one to prepare magnetic cobalt layers with a specific type of the magnetization behavior due to redistribution of cobalt magnetic phases. In summary, we note that the obtained experimental results are important not only for testing the technology of fabricating magnetic films applicable in devices of functional electronics. They relate the technologic regime and structural features of semiconductor structures with the film magnetic characteristics.

The results of investigations of the interlayer interactions will be presented in another article.

ACKNOWLEDGMENTS

We are grateful to D.A. Marushchenko for performing investigations on an atomic force microscope.

This study was supported by the Russian Foundation for Basic Research (project no. 11-02-00675-a).

REFERENCES

1. I. Žubić, J. Fabian, and S. Das Sarma, Rev. Mod. Phys. **76**, R323 (2004).
2. S. Toscano, B. Briner, H. Hopster, and M. Landolt, J. Magn. Magn. Mater. **114**, L6 (1992).
3. B. Briner and M. Landolt, Phys. Rev. Lett. **73**, R340 (1994).

4. G. S. Patrin, N. V. Volkov, and V. P. Kononov, JETP Lett. **68** (4), 307 (1998).
5. G. S. Patrin, N. V. Volkov, S. G. Ovchinnikov, E. V. Eremin, M. A. Panova, and S. N. Varnakov, JETP Lett. **80** (7), 491 (2004).
6. G. S. Patrin, V. O. Vas'kovskii, D. A. Velikanov, A. V. Svalov, and M. A. Panova, Phys. Lett. A **309**, R155 (2003).
7. V. O. Vas'kovskii, G. S. Patrin, D. A. Velikanov, A. V. Svalov, and N. N. Shchegoleva, Low Temp. Phys. **33** (4), 324 (2007).
8. J. Decoster, H. Bemelmans, S. Degroote, R. Moons, J. Verheyden, A. Vantomme, and G. Langouche, J. Appl. Phys. **81**, 5349 (1997).
9. C. P. Slichter, *Principles of Magnetic Resonance* (Springer-Verlag, Berlin, 1980).
10. G. I. Frolov, V. S. Zhigalov, and V. K. Mal'tsev, Phys. Solid State **42** (2), 334 (2000).
11. G. S. Patrin, C.-G. Lee, I. A. Turpanova, S. M. Zharkov, D. A. Velikanov, V. K. Maltsev, L. A. Li, and V. V. Lantsev, J. Magn. Magn. Mater. **306**, R218 (2006).
12. G. S. Patrin, Chan-Gyu Lee, Bon-Heun Koo, and Keesam Shin, Phys. Lett. A **359**, 149 (2006).
13. D. Sander, J. Phys.: Condens. Matter **16**, R603 (2004).

Translated by Yu. Ryzhkov